Nanoscale Horizons

COMMUNICATION

View Article Online
View Journal | View Issue

Cite this: *Nanoscale Horiz.*, 2018, 3, 335

Received 5th December 2017,
Accepted 30th January 2018

DOI: 10.1039/c7nh00197e

rsc.li/nanoscale-horizons

MBene (MnB): a new type of 2D metallic ferromagnet with high Curie temperature†

Zhou Jiang, Peng Wang, Xue Jiang * and Jijun Zhao

We extend the 2D MXene family into the boride world, namely, MBenes. High-throughput calculations screen twelve MBenes with excellent stability. Among them, 2D MnB MBene exhibits robust metallic ferromagnetism (~3.2 μ_B per Mn atom) and high Curie temperature (345 K). After functionalization with the –F and –OH groups, the ferromagnetic ground state of 2D MnB is well preserved. The Curie temperature is increased to 405 and 600 K, respectively, providing a novel and feasible strategy to tailor the T_C of 2D magnetic materials.

Conceptual insights

MXenes exfoliated from bulk MAX phases have emerged as promising 2D materials. Inspired by recently fabricated crystalline ternary borides (MAB phases), we extend the MXene family into the boride world, namely MBenes. From *ab initio* high-throughput search, we identify twelve stable MBene sheets that may exist in reality. Among them, the MnB sheet exhibits robust metallic ferromagnetism and high Curie temperature, making it a promising candidate for spintronics. Remarkably, with the help of the –F and –OH functional groups on the surface, the ferromagnetic ground state can be well preserved and the Curie temperature is even increased by up to 255 K. The thermal and mechanical stabilities of the MnB sheet have been confirmed and its possible mechanical exfoliation from bulk ternary borides has also been assessed by ideal fracture strength. Once the predicted MnB and other MBene sheets are synthesized, they would open a new avenue for 2D materials and devices.

1. Introduction

Graphene, owing to its flat structure and high surface area, holds great promise for applications in electronics, magnetics, optics, optoelectronics, thermoelectrics, catalysts, and energy storage systems.[1,2] The boom of graphene has stimulated the discovery and fabrication of a wealth of other two-dimensional (2D) materials.[3] Transition metal carbides, nitrides and carbides/nitrides (namely, MXenes) are attractive additions to the 2D family. MXenes are mainly produced by selectively etching the atomic layers from their layered parents of bulk MAX phases. MAX phases are named according to their compositions, where M is a transition metal, A is an element mostly in the IIIA and IVA columns, and X is carbon or nitrogen.[4] So far, more than 70 MXenes have been theoretically predicted and 19 of them have been experimentally synthesized.[5] Applications of MXenes in field effect transistors,[6] Li ion batteries,[7] catalysts,[8] and photocatalysts[9] have been explored. Even with such a wide variety of MXenes, an intriguing question arises: whether X can be extended to the other elements?

Boron is the fifth element in the periodic table and its number of valence electrons is only one/two less than carbon/nitrogen. Its electron deficiency, electronegativity, and atomic size would endow 2D boron materials with distinctly different properties from other 2D materials. For instance, most elementary 2D materials are graphene analogues with flat or buckled honeycomb structures, while borophene has a triangular lattice with different arrangements of hexagonal holes.[10,11] The biggest challenge for the synthesis of boron based 2D materials is surplus electron balance, which can be solved by hexagonal hole introduction[12,13] and metal substrate passivation.[14,15] Another practical method to realize 2D boron based systems is the combination between boron and various transition metals. On one hand, the transition metal would donate electrons to boron to stabilize the boron sheet. On the other hand, the highly coordinated transition metal center may impart novel complexity and diversity to 2D boride materials.

Among transition metal borides, only magnesium diboride[16] and titanium diboride[17] sheets have been synthesized by exfoliation through ultrasonication and intercalation of alkali metals. However, the conventional chemical etching method to produce

Key Laboratory of Materials Modification by Laser, Ion and Electron Beams (Dalian University of Technology), Ministry of Education, Dalian 116024, China. E-mail: jiangx@dlut.edu.cn

† Electronic supplementary information (ESI) available: Geometries, phonon band structures and other details for twelve MBenes (MnB, HfB, ZrB, Au_2B, Mo_2B, Nb_5B_2, Nb_3B_4, Ta_3B_4, V_3B_4, OsB_2, FeB_2, and RuB_2), AIMD simulation results, spin-polarized band structures (PBE and HSE06 methods), four magnetic configurations of a MnB sheet and its functionalized structural forms (MnBF and MnBOH) with their corresponding densities of states. See DOI: 10.1039/c7nh00197e

MXenes from the corresponding MAX phases has not been reported for 2D transition metal borides. This is mainly limited by the lack of ternary borides having layered crystal structures with easily etchable layers. Recently, MAX analogues, a series of single crystalline ternary borides (MAB phases), have been successfully fabricated, including Cr_2AlB_2, Cr_3AlB_4, Cr_4AlB_6, WAlB, MoAlB, Mn_2AlB_2, and Fe_2AlB_2.[18] These structures are composed of aluminium layers that are suitable to generate 2D transition metal borides, as demonstrated in previous studies on MXenes.[4,19–21] Since these 2D transition metal borides originate from the ternary borides, we name them as MBenes. If any of the MBenes can be verified in experiment, the richness of boron chemistry would open a new avenue with diverse applications. Then it is natural to ask: is it possible to obtain 2D MBenes from MAB phases?

To address this question, here we present *ab initio* high-throughput calculations to search for potential 2D MBene candidates. From an analysis of the database of binary borometallic molecules, twelve 2D borides (MnB, HfB, ZrB, Au_2B, Mo_2B, Nb_5B_2, Nb_3B_4, Ta_3B_4, V_3B_4, OsB_2, FeB_2, and RuB_2) stand out for their satisfactory stability. Among them, 2D metal MnB MBene exhibits robust ferromagnetism (FM). Remarkably, its metallic behavior, ferromagnetic state and high Curie temperature are well retained even after functionalization with the –F or –OH groups. As the first attempt to extend MXenes into boride systems, our findings not only enrich the possible diversity of 2D materials in theory but also bring about new opportunities of spintronic applications.

2. Computational details

Our calculations were carried out using spin-polarized density functional theory (DFT) within the generalized gradient approximation (GGA)[22] as implemented in the Vienna Ab initio Simulation Package (VASP),[23,24] with the Perdew–Burke–Ernzerhof (PBE) exchange–correlation functional. The projected augmented wave (PAW) approach was used to describe the ion–electron interaction.[25,26] To appropriately account for the strongly correlated electrons, the GGA+*U* method was used to deal with the partially filled d orbitals of the Mn atoms.[27] For the Mn 3d-orbitals, the effective on-site Coulomb interaction parameter (U) and the exchange interaction parameter (J) were set to 3 eV and 1 eV, respectively. The choice of U and J values was carefully tested by optimizing the lattice parameters of Mn_2AlB_2 and Mn_4B_4, and the results are given in Table S1 (ESI†). The energy cutoff of the plane-wave basis was 650 eV. During geometry optimization, numerical convergence was achieved with a tolerance of 10^{-6} eV in energy and 0.001 eV Å^{-1} in force, respectively. To avoid interaction between a layer and its replica, a large vacuum space of 16 Å was added along the z axis. The Brillouin zone was sampled with a 19 × 19 × 1 Monkhorst–Pack k-point grid for geometry optimization and a set of 23 × 23 × 1 grids for electronic structure calculations. For the equilibrium MBene structures, their phonon dispersions were computed using the direct supercell method as implemented in the Phonopy program.[28] Ab initio molecular dynamics (AIMD) simulations were also performed to assess the thermal stability of the 2D MnB structure and its functionalized forms (MnBF and MnBOH) at 600 K, 900 K and 1200 K, respectively.

3. Results and discussion

A high-throughput structural search was carried out to identify the stable structures of 2D transition metal borides M_xB_y, where M stands for transition metals in 3d (Ti, V, Cr, Mn, Fe, Co, Ni, Cu and Zn), 4d (Zr, Nb, Mo, Tc, Ru, Rh, Pd, Ag and Cd) and 5d (Hf, Ta, W, Re, Os, Ir, Pt, Au and Hg), and the $x:y$ ratios are 1 : 2, 3 : 4, 1 : 1, 2 : 1, and 5 : 2. Among them, we identified twelve unprecedented 2D MBenes, including MnB, HfB, ZrB, Au_2B, Mo_2B, Nb_5B_2, Nb_3B_4, Ta_3B_4, V_3B_4, OsB_2, FeB_2, and RuB_2. Their crystalline structures are displayed in Fig. S1(a) (ESI†). The cohesive energies, bond lengths, and slice thicknesses are listed in Table S2 (ESI†). The cohesive energy is defined as

$$E_{coh} = (xE_M + yE_B - E_{MxBy})/(x + y),$$

where E_M and E_B are the total energies of an isolated transition metal and the B atom, respectively; E_{MxBy} is the total energy of the unit cell of the TMB sheet. The average values of these cohesive energies are 6.08 eV per atom, which is comparable to common 2D layered materials like MoS_2 (5.02 eV per atom), $g_{1/8}$ borophene sheets (5.81 eV per atom) and Mo_2C (5.98 eV per atom). Their dynamic stabilities were further assessed in terms of phonon band structures (Fig. S1(b), ESI†), and no imaginary frequencies were observed throughout the entire Brillouin zone. Both satisfactory cohesive energy and phonon dispersion imply that those 2D MBene candidates are thermodynamically and dynamically stable. Among these twelve systems, 2D MnB MBene possesses the largest magnetic moments (Table S1, ESI†), which arouse our interest in exploring its other properties further.

Fig. 1(a) presents the optimized structure of a 2D MnB sheet. Its unit cell with lattice constants a = 2.881 Å and b = 2.932 Å contains two Mn atoms and two B atoms. Unlike common hexagonal 2D materials such as graphene,[29] silicene[30] MoS_2[31] and Ti_3C_2,[20] the 2D MnB sheet shows a rectangular lattice with the space group *Pmma* (No. 51), leading to anisotropy in the x and y directions. Each Mn or B atom forms six bonds with its neighbouring atoms, with a bilayer buckled structure with Mn atoms on the upmost surfaces and the distance between Mn layers being h = 2.125 Å. The intralayer Mn–B bond length is 2.119 Å (d_1) and the interlayer one is 2.176 Å (d_2). Due to the electron deficiency of boron, the Mn–B bond in MnB is slightly weaker than those in Mn_2C[32] and MnN_2[33] where the Mn–C and Mn–N bond lengths are 1.956 and 1.949 Å, respectively. Note that in the database of binary boron compounds[34] such borides with one dimensional zigzag chains have also been observed in bulk MnB, CrB, and MoB crystals. Our proposed 2D MnB is different from them in terms of the relative position of parallel zigzag chains formed by Mn atoms. This unique configuration suggests that the MnB sheet exhibits distinct physical and chemical properties.

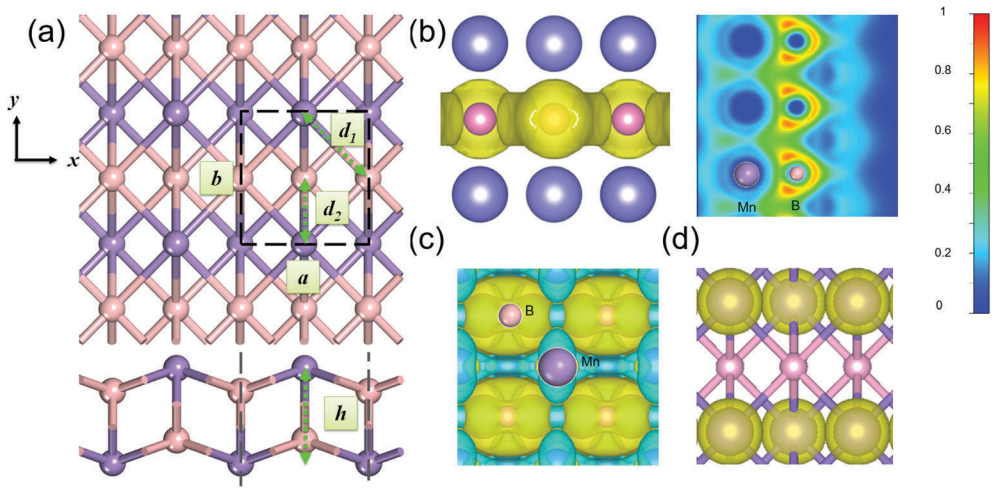

Fig. 1 (a) Top and side views of a 2D MnB sheet; *a* and *b* are the lattice parameters, and *h* denotes the thickness of the layer. (b) Maps of the electron localization function (ELF) located on the (0 −1 −6) plane with a scale bar from 0 to 1. (c) The deformation density of the MnB sheet with an isosurface of 0.01 e Å^{-3}. The yellow and cyan regions represent the accumulation and depletion of electrons, respectively. (d) The spin polarization distribution with an isosurface of 0.75 e Å^{-3}. The yellow color indicates a net spin-up polarization, and the spin polarization is mainly on the Mn sites.

The calculated cohesive energy of the MnB sheet is 4.80 eV per atom, which is slightly lower than that of a bulk MnB crystal (5.35 eV) and higher than that of the recently proposed Mn-containing MXene phases such as Mn_2C (4.42 eV per atom) and MnN_2 (3.45 eV per atom). From our calculations, the 2D elastic constants of C_{11}, C_{12}, C_{22}, and C_{44} are 197, 50, 158 and 90 N m^{-1}, respectively, satisfying the Born–Huang stability criteria[35] and confirming that the MnB layer is mechanically stable. To further check its thermal stability, we used a relatively large 4 × 4 supercell to carry out AIMD simulations within the canonical ensemble (*NVT*) at temperatures of 300, 600, and 1200 K, respectively. Up to 1200 K, no severe geometrical reconstructions are observed after 20 ps (Fig. S2(a), ESI†) and the average displacement of Mn atoms is about 0.08 Å, which means that the framework of Mn atoms basically remains unchanged.

To explain the origin of high stability and gain deep insight into the bonding character, we calculated the electron localization function (ELF). The homogeneous electron gas is renormalized to values from 0.0 to 1.0, shown in different colours. By definition, the region with a value of 1.0 indicates perfect electron localization, 0.5 represents a fully delocalized electron, and the region with a value close to 0.0 refers to very low charge density.[22] From Fig. 1(b), one can clearly see that the ELF for the region around Mn atoms is 0.0, indicating their electron deficiency. At the same time, the B frameworks are fully surrounded by homogeneous electron gas (ELF = 0.5), which is crucial to stabilize the entire 2D sheet *via* strong B–B bonds. Bader charge analysis shows that each Mn atom donates approximately 0.68 electron to each B atom within the MnB sheet, reflecting the nature of Mn–B ionic bonding. This can be understood by the electronegativities of B (2.04) and Mn (1.55). The electron transfer from Mn to B further contributes to the high stability of the 2D MnB system. As shown in Fig. 1(c), the deformation electron density (DED) also verifies the above bonding characteristics. The transferred electrons are mostly accumulated around the B sites, in agreement with the ELF analysis.

Considering its high stability, it is natural to wonder how the MnB sheet can be synthesized in experiments. There are three feasible pathways to support our hypothetical 2D MnB sheet. Firstly, the Mo_2C MXene was prepared with the traditional chemical vapour deposition (CVD) method,[36] which is commonly used for growing graphene, MoS_2, and many other 2D materials. Thus, monolayer transition borides might also be fabricated using CVD growth. Secondly, the ternary layered phase Mn_2AlB_2 has already been synthesized by arc-melting.[18] The corresponding MnB sheet can be produced by selective chemical etching of the Al metal layer. Such a method has been successfully employed to convert 3D MAX phases Ti_2AlC, Nb_2AlC, V_2AlC, and $(Ti_{0.5}Nb_{0.5})AlC$ to 2D MXene phases of Ti_2C, Nb_2C, V_2C, and $(Ti_{0.5}Nb_{0.5})C$, respectively.[19] Thirdly, one can also attempt to mechanically exfoliate MBenes from MAB phases. To further confirm the possibility, we investigated the tensile deformation mechanism of Mn_2AlB_2. Both the stress–strain curves and ELF counter plots (Fig. 2) show that when the tensile strain increases from 1% to 30% along the *z* axis the strengths of the B–Mn bonds remain unchanged, while the Mn–Al bonds are significantly weakened as electrons are localized

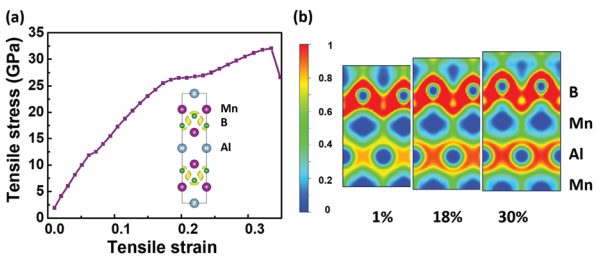

Fig. 2 (a) The calculated stress–strain curve of Mn_2AlB_2 with the ELF contour plots and (b) projected on the plane containing Mn and Al atoms under [0001] tensile strains of 1%, 18%, and 30%.

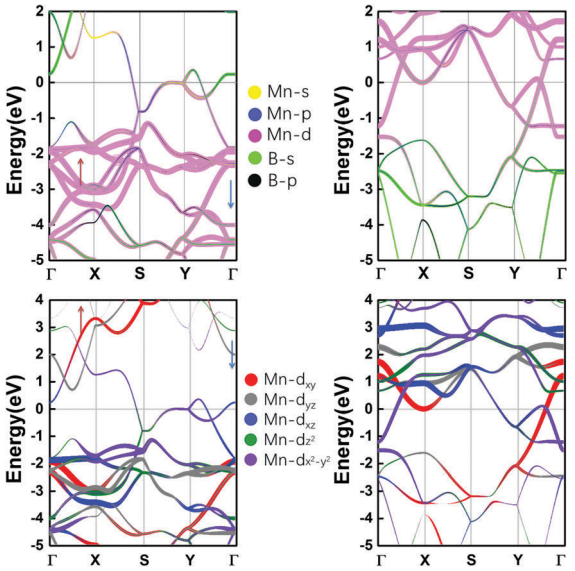

Fig. 3 Atom-projected and orbital-projected band structures of MnB sheets in spin-up and spin-down channels, and the Fermi levels are set to zero.

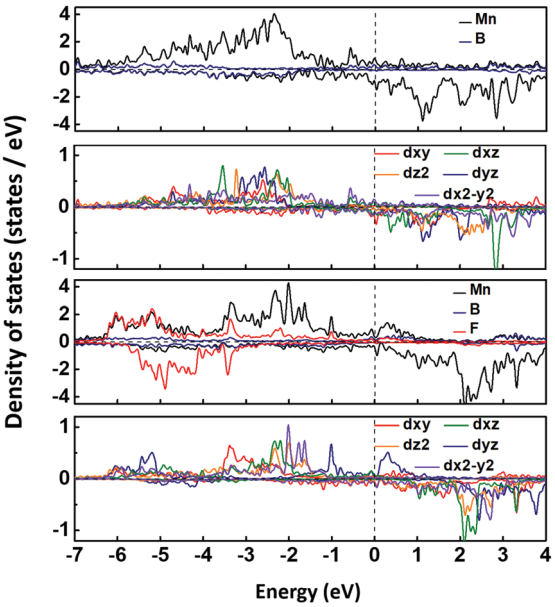

Fig. 4 Atom-projected and orbital-projected densities of states for MnB and MnBF sheets, and the Fermi levels are all set to zero.

around Al atoms. This implies that the MnB layers are likely to be separated from the Al layers *via* Mn–Al bond breaking. In addition, the ideal fracture strength for mechanical exfoliation is as low as 32 GPa, which is comparable to the values of W_2AlC (36 GPa), Cr_2AlC (35 GPa), Mo_2AlC (34 GPa), Ta_2AlC (32 GPa), and V_2AlC (32 GPa).[37] This implies that mechanically exfoliating MnB layers from a Mn_2AlB_2 crystal is feasible.

The spin-polarized band structures in Fig. S3 (ESI†) show that the MnB sheet is metallic with several partially occupied bands crossing the Fermi level in both spin channels. The metallicity is further confirmed by the result of computations using the HSE06 functional.[38] Moreover, the atom-projected and orbital-projected bands in Fig. 3 demonstrate that the metallicity is derived from Mn-3d orbitals (Mn-d_{xy}, $d_{x^2-y^2}$, d_{xz}) and B-p orbitals near the Fermi energy. As listed in Table 1, the total magnetic moment of 6.04 μ_B per unit cell is mainly contributed by Mn atoms, which is intuitively shown in the spin-density distribution in Fig. 1(d). Each Mn atom has an on-site moment of 3.2 μ_B and the spin moments of boron atoms (-0.18 μ_B) align antiferromagnetically. To further clarify the origin of magnetic moments, Fig. 4 shows the atom-projected and Mn-3d orbital-projected densities of states. It is clear that Mn-3d orbitals (d_{yz}, d_{xz}, $d_{x^2-y^2}$) are fully occupied in spin-up states, while the d_{xy} and d_{z^2} orbitals are partially filled in both up and down spin channels. Mn's five d orbitals have non-degenerate energies, which originate from the B induced asymmetric octahedral crystal field around Mn atoms. The strong hybridization between B-p orbitals and Mn-d orbitals is responsible for such a phenomenon. Hence, the electronic structure of MnB can be expected for a formal Mn^{3+} electronic configuration in a high spin state with three unpaired d electrons ($d^{3\uparrow}$ spin configuration). The atom- and orbital-projected electronic band structure analyses (Fig. 3) also confirm the p–d hybridization and the difference in the dispersions in the two spin channels associated with the crystal field splitting.

In order to further explore the preferred magnetic interaction, we optimized a 2 × 2 MnB supercell and considered four possible magnetic configurations (Fig. S4, ESI†): one ferromagnetic (FM) and three antiferromagnetic (AFM). The exchange energy is defined as $E_{ex} = (E_{AFM} - E_{FM})$ per Mn_8B_8 formula unit, where E_{AFM} and E_{FM} are the energies of the Mn atoms with AFM and FM coupling in the 2 × 2 MnB sheet. The calculated energy differences between these magnetic configurations are summarized in Table 2. For the MnB sheet, the FM ground state is more stable than the AFM states by at least 180 meV per Mn_8B_8 formula unit. As discussed above, the indirect p–d exchange interaction plays an important role in the ferromagnetic coupling of MnB sheets.

One important quantity of ferromagnetism is the Curie temperature (T_C) corresponding to the transition from the ferromagnetic to paramagnetic phase. For practical spintronic

Table 1 Atomic charge differences (electrons per atom) obtained from Bader charge analysis (positive and negative values indicate electron gain and loss, respectively), and the atomic and orbital magnetic moments (M) of MnB, MnBX (X = F or OH). M_T represents the total magnetic moment

System	Q_{Mn}/e	Q_B/e	Q_X/e	M_{Mn}/μ_B	$M_{Mn\text{-}d}/\mu_B$	M_B/μ_B	$M_{B\text{-}p}/\mu_B$	M_X/μ_B	M_T/μ_B
MnB	−0.68	0.68	—	3.20	3.15	−0.18	−0.15	—	6.04
MnBF	−1.10	0.51	0.59	3.24	3.20	−0.20	−0.16	0.06	6.20
MnBOH	−1.10	0.50	0.60	3.15	3.11	−0.20	−0.16	0.07	6.04

Table 2 Calculated energies of the ferromagnetic state (E_{FM}) and antiferromagnetic states (E_{AFM}), the energy differences (ΔE) between E_{AFM} and E_{FM} for the Mn_8B_8 formula unit and the magnetic moments (M_{total}) of all states

	E_{Total}/eV	ΔE/meV	M_{total}/μ_B
FM	−108.697	0	25.46
AFM1	−108.198	499	0
AFM2	−108.218	479	0
AFM3	−108.517	180	0

applications, T_C above room temperature is desirable. Here T_C is estimated using the 2D Heisenberg model, where the Hamiltonian operator can be written as

$$H = -\sum_{i,j} J_1 M_i M_j - \sum_{k,l} J_2 M_k M_l - \sum_{p,q} J_3 M_p M_q,$$

where M_i is the magnetic moment at site I and J is the exchange coupling parameter (J_1, J_2 and J_3 stand for the nearest, second-nearest, and third-nearest site pairs). From the distances between the nearest, second-nearest, and third-nearest Mn atoms of 2.567, 2.881 and 2.932 Å, respectively, the calculated exchange coupling parameters J_1, J_2 and J_3 are 3.1, 1.4 and −2.3 meV (details are in the ESI,† S4). Within mean field theory (MFT), the estimated T_C is in the 258–418 K range. It is known that MFT cannot accurately describe the magnetic percolation effect and tends to overestimate T_C. Therefore, we evaluated the T_C of the MnB sheet by using Monte Carlo (MC) simulation based on the 2D Ising model of a 100 × 100 supercell, and the simulation lasted for 1.2 × 10^5 iterations. The temperature-dependent magnetic moment for the MnB sheet is plotted in Fig. 5, showing that the magnetic moment falls drastically at T_C ~ 345 K. Compared with the above estimation with MFT, T_C is reduced by 17%. Even so, it is still higher than room temperature and those of many previously reported 2D magnetic materials such FeC_2 (245 K),[39] MnO_2 (140 K),[40] Cr@gt-C_3N_3 (325 K),[41] MnPc (150 K)[42] and Nb_3Cl_8 (31 K).[43] Moreover, the T_C value for MnB is significantly higher than the highest T_C value (110 K) achieved experimentally in a Mn-doped GaAs monolayer.[44]

The magnetic anisotropy energy (MAE) is an important property for high density storage and quantum spin processing. In principle, reducing dimensionality and symmetry would increase MAE relative to the corresponding 3D bulk phase. For the MnB sheet, the easy magnetization axis is the z direction (out-of-plane), along which the magnetization energy is lower than those along the x- and y-directions by 25 and 175 μeV per Mn atom, respectively. These MAE values are comparable to those of reported 2D material Mn_2C (25 μeV)[32] and bulk Co (65 μeV per Co atom), and are one order of magnitude higher than those of bulk Fe (1.4 μeV per atom) and Ni (2.7 μeV per atom).[45] The sizeable MAEs make the MnB sheet potentially useful for magnetoelectronic applications.

Considering that a bare MnB sheet is chemically active and could be exfoliated and terminated with the –F and –OH groups in experiment,[19] we further exploited the influence of these functional groups on the structural, electronic and magnetic properties of the MnB sheet. As representatives, we considered two functionalized species, *i.e.*, MnBF and MnB(OH). As shown in Fig. S5 (ESI†), three possible configurations are considered for each MnB sheet, where the functional groups are placed at the top sites of B atoms (H_1), hollow sites of Mn atoms (H_2), and hollow sites of B atoms (H_3). We find that both the –OH and –F functional groups are most energetically favorable at the hollow site B atoms (H_3) on both sides. This is understandable since the Mn atoms are the electron donor and the functional groups are more likely to bond with Mn atoms than B atoms. Indeed, significant electron transfer (Table 1) from the Mn-3d orbitals to the –F and –OH functional groups has been observed in MnBF and MnB(OH) by 0.59 e and 0.60 e, respectively, in addition to the electron transfer from Mn to B by 0.5 e on average, whereas no electron transfer was seen between the B atoms and F- and OH- functional groups. As a consequence, such charge transfer slightly elongated the Mn–B bonds; that is, the average Mn–B bond lengths of the OH-terminated and F-terminated MnB sheets are 2.223 Å, and 2.239 Å, respectively. Our AIMD simulations of MnBF and MnBOH indicate that both of them are thermally stable at 600 K after 20 ps (Fig. S2(b), ESI†).

We further investigated the electronic and magnetic properties of those functionalized MnB. Both MnB derivatives still exhibit metallic behavior, as clearly seen from the spin-polarized electronic band structures in Fig. 6. More importantly, the magnetic ground state and magnetic moments on the Mn atoms are well retained after functionalization (Table 1). For MnBF and MnB(OH), the FM

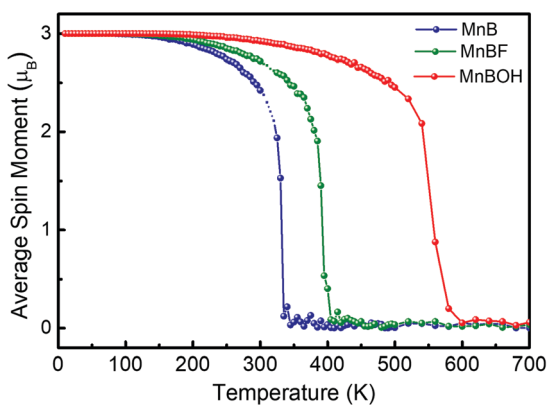

Fig. 5 On-site magnetic moment of Mn atoms *versus* temperature in MnB (blue), MnBF (green), MnBOH (red) sheets.

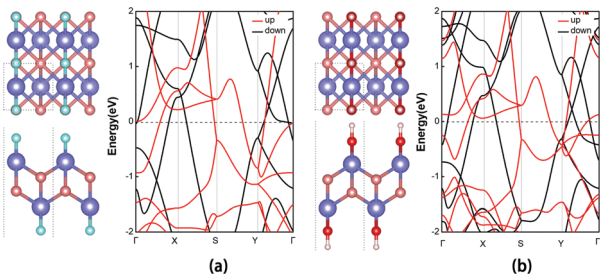

Fig. 6 (a and b) Side and top views of MnBX (X = F or OH) structural forms and the corresponding spin-polarized band structures.

Table 3 Comparison of magnetic moments (M), energy differences (ΔE for a 2 × 2 supercell), and T_C estimated using the MFA method and MC simulation for MnB and MnBX (X = F or OH), respectively

	M_T/μ_B	M_{Mn}/μ_B	ΔE/meV	T_C (MFA)/K	T_C (MC)/K
MnB	6.04	3.20	180	217–347	345
MnBF	6.20	3.24	340	618–989	405
MnBOH	6.04	3.15	77	333–532	600

state is more stable than the AFM state by 340 meV and 77 meV per 2 × 2 supercell, respectively (Table 3). At the same time, the on-site magnetic moments on Mn atoms are 3.20, 3.24, and 3.15 μ_B for MnB, MnBF, and MnB(OH), respectively. The total and orbital-projected densities of states of MnB and MnBF sheets are shown in Fig. 4. The almost unchanged magnetic behavior is closely related to the highly split d orbitals of Mn atoms. Initially, the d_{yz} orbitals in the spin-up channel are occupied, while the $d_{x^2-y^2}$ orbitals partially occupy the spin-down channel. Upon functionalization, the d_{yz} orbitals in the spin-up channel become partially occupied, while the $d_{x^2-y^2}$ orbitals in the spin-up channel become fully occupied. This results in a robust magnetic moment of ~3 μ_B per Mn atom for both MnB and MnBF sheets. A similar picture is applicable to the case of the MnBOH system, and the PDOS is shown in Fig. S6 (ESI†).

The Curie temperatures of MnBF and MnBOH sheets are then estimated by the MFA method and MC simulation, and the results are listed in Table 1. Fig. 5 shows that the T_C is further increased up to 405 K (MC) and 600 K (MC) through F- and OH- functionalization. Note that this value is also comparable to the calculated high T_C of a functionalized Mn-based 2D system, *i.e.*, Mn_2CF_2 (520 K).[46] Owing to its insensitive metallic behavior, robust FM state and high Curie temperature, the MnB sheet is superior to most reported 2D MXene materials.[47] Taking Ti_2C as an example, the magnetic moment of Ti_2C is 0.982 μ_B per atom. However, upon functionalization, the magnetism is quenched, which strongly limits its practical application in spintronics. More excitingly, our results suggest that chemical functionalization is an effective method to tailor T_C for 2D magnetic materials. In the present situation, the Curie temperatures of MnBF and MnB(OH) are 60 and 255 K higher than those of the pristine MnB sheet.

4. Conclusions

In summary, motivated by the recent experimentally obtained 3D MAB phases, we explored the geometrical, electronic, and magnetic properties of their 2D MBene analogues. Taking MnB as an example, exfoliation from a 3D crystal to a 2D layer is feasible, as confirmed by its low fracture strength, and high thermal, dynamic, and mechanical stabilities. The 2D MnB MBene sheet and its functionalized products exhibit metallic ferromagnetic behavior with the Curie temperature above room temperature (345–600 K). The ferromagnetism and metallicity mainly arise from the p–d hybridization mechanism and crystal field splitting. Importantly, the characteristic of the high temperature ferromagnetic metal is insensitive to their chemical functionalization. These advantages make 2D MnB MBene a promising material for spintronic devices. Like MXene, transition metal borides can lead to many possible 2D binary compounds; *e.g.*, MnB, HfB, ZrB, Au_2B, Mo_2B, Nb_5B_2, Nb_3B_4, Ta_3B_4, V_3B_4, OsB_2, FeB_2, and RuB_2 sheets are predicted as potential metastable phases. Their fruitful applications will be reported in our future study. Our first successful attempt to extend MXenes into boride systems would significantly promote the diversity of 2D materials and encourage scientists to design and synthesize those interesting 2D MBene materials in the future.

Conflicts of interest

There are no conflicts to declare.

Acknowledgements

This work was supported by the National Natural Science Foundation of China (11404050, 11574040) and the Fundamental Research Funds for the Central Universities of China (DUT16RC(4)50, DUT16JJ(G)05, DUT16LAB01, DUT17LAB19). We also acknowledge the Supercomputing Center of the Dalian University of Technology for providing the computing resource.

Notes and references

1 J. Pan, S. Lany and Y. Qi, *ACS Nano*, 2017, **11**, 7560–7564.
2 M. Khazaei, A. Ranjbar, M. Arai, T. Sasaki and S. Yunoki, *J. Mater. Chem. C*, 2017, **5**, 2488–2503.
3 S. Z. Butler, S. M. Hollen, L. Cao, Y. Cui, J. A. Gupta, H. R. Gutierrez, T. F. Heinz, S. S. Hong, J. Huang, A. F. Ismach, E. Johnston-Halperin, M. Kuno, V. V. Plashnitsa, R. D. Robinson, R. S. Ruoff, S. Salahuddin, J. Shan, L. Shi, M. G. Spencer, M. Terrones, W. Windl and J. E. Goldberger, *ACS Nano*, 2013, **7**, 2898–2926.
4 M. Naguib, O. Mashtalir, J. Carle, V. Presser, J. Lu, L. Hultman, Y. Gogotsi and M. W. Barsoum, *ACS Nano*, 2012, **6**, 1322.
5 B. Anasori, M. R. Lukatskaya and Y. Gogotsi, *Nat. Rev. Mater.*, 2017, **2**, 16098.
6 S. Lai, J. Jeon, S. K. Jang, J. Xu, Y. J. Choi, J. H. Park, E. Hwang and S. Lee, *Nanoscale*, 2016, **8**, 1216.
7 Q. Tang, Z. Zhou and P. Shen, *J. Am. Chem. Soc.*, 2012, **134**, 16909–16916.
8 G. Fan, X. Li, Y. Ma, Y. Zhang, J. Wu, B. Xu, T. Sun, D. Gao and J. Bi, *New J. Chem.*, 2017, **41**, 2793–2799.
9 Z. Guo, J. Zhou, L. Zhu and Z. Sun, *J. Mater. Chem. A*, 2016, **4**, 11446–11452.
10 A. J. Mannix, X. F. Zhou, B. Kiraly, J. D. Wood, D. Alducin, B. D. Myers, X. Liu, B. L. Fisher, U. Santiago, J. R. Guest, M. J. Yacaman, A. Ponce, A. R. Oganov, M. C. Hersam and N. P. Guisinger, *Science*, 2015, **350**, 1513–1516.
11 B. Feng, J. Zhang, Q. Zhong, W. Li, S. Li, H. Li, P. Cheng, S. Meng, L. Chen and K. Wu, *Nat. Chem.*, 2016, **8**, 563–568.
12 H. Tang and S. Ismail-Beigi, *Phys. Rev. Lett.*, 2007, **99**, 115501.
13 X. Wu, J. Dai, Y. Zhao, Z. Zhuo, J. Yang and X. C. Zeng, *ACS Nano*, 2012, **6**, 7443–7453.

14 Y. Liu, E. S. Penev and B. I. Yakobson, *Angew. Chem., Int. Ed. Engl.*, 2013, **52**, 3156–3159.
15 H. Liu, J. Gao and J. Zhao, *Sci. Rep.*, 2013, **3**, 3238.
16 C. Cepek, R. Macovez, M. Sancrotti, L. Petaccia, R. Larciprete, S. Lizzit and A. Goldoni, *Appl. Phys. Lett.*, 2004, **85**, 976–978.
17 G. Hilz and H. Holleck, *Int. J. Refract. Met. Hard Mater.*, 1996, **14**, 97–104.
18 P. Chai, S. A. Stoian, X. Tan, P. A. Dube and M. Shatruk, *J. Solid State Chem.*, 2015, **224**, 52–61.
19 M. Naguib, V. N. Mochalin, M. W. Barsoum and Y. Gogotsi, *Adv. Mater.*, 2014, **26**, 992–1005.
20 M. Naguib, M. Kurtoglu, V. Presser, J. Lu, J. Niu, M. Heon, L. Hultman, Y. Gogotsi and M. W. Barsoum, *Adv. Mater.*, 2011, **23**, 4248–4253.
21 M. Ghidiu, M. Naguib, C. Shi, O. Mashtalir, L. M. Pan, B. Zhang, J. Yang, Y. Gogotsi, S. J. Billinge and M. W. Barsoum, *Chem. Commun.*, 2014, **50**, 9517–9520.
22 J. P. Perdew, K. Burke and M. Ernzerhof, *Phys. Rev. Lett.*, 1997, **77**, 3865.
23 G. Kresse and J. Furthmuller, *Phys. Rev. B: Condens. Matter Mater. Phys.*, 1996, **54**, 11169–11186.
24 G. Kresse and J. Furthmuller, *Comput. Mater. Sci.*, 1996, **6**, 15–50.
25 P. E. Blöchl, *Phys. Rev. B: Condens. Matter Mater. Phys.*, 1994, **50**, 17953–17979.
26 G. Kresse and D. Joubert, *Phys. Rev. B: Condens. Matter Mater. Phys.*, 1999, **59**, 1758–1775.
27 A. I. Liechtenstein, V. I. Anisimov and J. Zaanen, *Phys. Rev. B: Condens. Matter Mater. Phys.*, 1995, **52**, R5467–R5470.
28 K. Parlinski, Z. Q. Li and Y. Kawazoe, *Phys. Rev. Lett.*, 1997, **78**, 4063–4066.
29 K. S. Novoselov, D. Jiang, F. Schedin, T. J. Booth, V. V. Khotkevich, S. V. Morozov and A. K. Geim, *Proc. Natl. Acad. Sci. U. S. A.*, 2005, **102**, 10451–10453.
30 J. Zhao, H. Liu, Z. Yu, R. Quhe, S. Zhou, Y. Wang, C. C. Liu, H. Zhong, N. Han, J. Lu, Y. Yao and K. Wu, *Prog. Mater. Sci.*, 2016, **83**, 24–151.
31 H. Shu, F. Li, C. Hu, P. Liang, D. Cao and X. Chen, *Nanoscale*, 2016, **8**, 2918–2926.
32 L. Hu, X. Wu and J. Yang, *Nanoscale*, 2016, **8**, 12939–12945.
33 J. Liu, Z. Liu, T. Song and X. Cui, *J. Mater. Chem. C*, 2017, **5**, 727–732.
34 G. Akopov, M. T. Yeung and R. B. Kaner, *Adv. Mater.*, 2017, **29**, 1604506.
35 M. Born, K. Huang and M. Lax, *Am. J. Phys.*, 1954, **39**, 113–127.
36 C. Xu, L. Wang, Z. Liu, L. Chen, J. Guo, N. Kang, X. L. Ma, H. M. Cheng and W. Ren, *Nat. Mater.*, 2015, **14**, 1135–1141.
37 Z. Guo, L. Zhu, J. Zhou and Z. Sun, *RSC Adv.*, 2015, **5**, 25403–25408.
38 J. Heyd, G. E. Scuseria and M. Ernzerhof, *J. Chem. Phys.*, 2003, **118**, 8207–8215.
39 T. Zhao, J. Zhou, Q. Wang, Y. Kawazoe and P. Jena, *ACS Appl. Mater. Interfaces*, 2016, **8**, 26207–26212.
40 M. Kan, J. Zhou, Q. Sun, Y. Kawazoe and P. Jena, *J. Phys. Chem. Lett.*, 2013, **4**, 3382–3386.
41 I. Choudhuri, P. Garg and B. Pathak, *J. Mater. Chem. C*, 2016, **4**, 8253–8262.
42 J. Zhou and Q. Sun, *J. Am. Chem. Soc.*, 2011, **133**, 15113–15119.
43 J. Jiang, Q. Liang, R. Meng, Q. Yang, C. Tan, X. Sun and X. Chen, *Nanoscale*, 2017, **9**, 2992–3001.
44 F. Matsukura, H. Ohno, A. Shen and Y. Sugawara, *Phys. Rev. B: Condens. Matter Mater. Phys.*, 1998, **57**, R2037–R2040.
45 G. H. O. Daalderop, P. J. Kelly and M. F. H. Schuurmans, *Phys. Rev. B: Condens. Matter Mater. Phys.*, 1990, **41**, 11919–11937.
46 J. He, P. Lyu and P. Nachtigall, *J. Mater. Chem. C*, 2016, **4**, 11143–11149.
47 Y. Xie and P. R. C. Kent, *Phys. Rev. B: Condens. Matter Mater. Phys.*, 2013, **87**, 235441.